LETTER

doi:10.1038/nature13122

Geomagnetic fluctuations reveal stable stratification at the top of the Earth's core

Bruce Buffett[1]

Modern observations of the geomagnetic field reveal fluctuations[1–3] with a dominant period of about 60 years. These fluctuations are probably a result of waves in the liquid core[4], although the precise nature of the waves is uncertain. Common suggestions include a type of magnetic wave, known as a torsional oscillation[5], but recent studies[6] favour periods that are too short to account for a 60-year fluctuation. Another possibility involves MAC waves[7], which arise from the interplay between magnetic, Archimedes and Coriolis forces. Waves with a suitable period can emerge when the top of the core is stably stratified. Here I show that MAC waves provide a good description of time-dependent zonal flow at the top of the core[8], as inferred from geomagnetic secular variation[9]. The same wave motion can also account for unexplained fluctuations in the dipole field[10]. Both of these independent predictions require a 140-kilometre-thick stratified layer with a buoyancy frequency comparable to the Earth's rotation rate. Such a stratified layer could have a thermal origin[11,12], implying a core heat flow of about 13 terawatts. Alternatively, the layer could result from chemical stratification[13,14]. In either case, the existence of a stratified layer at the top of the core obscures the nature of flow deeper in the core, where the magnetic field is continually regenerated.

Evidence for a 60-year fluctuation in the geomagnetic field was first reported[1] more than 40 years ago. Subsequent studies[2,3] using longer records have confirmed the existence of a dominant 60-year period, and find evidence for a weaker 30-year fluctuation. Initial explanations appealed to torsional oscillations[5], which are nearly geostrophic motions in the form of fluid cylinders aligned with the rotation axis. The restoring force for wave motion is due to the component of the magnetic field that threads across the surface of the cylinders. A nominal 60-year period implies a relatively weak magnetic field of roughly 0.3 mT (refs 15 and 16). Stronger magnetic fields in numerical geodynamo models[17] imply shorter periods and recent observations[6] support the existence of torsional oscillations with periods of 4 to 6 years.

Longer-period waves are possible when the top of the fluid core is stably stratified[7]. The required ingredients for wave motion include fluid buoyancy, rapid rotation and a radial magnetic field that passes through the stratified layer. Figure 1 shows a schematic illustration of the associated fluid velocity. A radial component of flow V_r alters the distribution of fluid density in the stratified layer and induces a perturbation in pressure. Owing to the effects of rapid rotation, the pressure perturbation causes an azimuthal flow V_ϕ much like cyclonic flow around a pressure low in the atmosphere. Azimuthal flow is opposed by the presence of the radial magnetic field, which drives a weaker meridional flow V_θ towards the pole. The restoring force for the waves comes partly from the buoyancy force, which opposes the radial motion, and partly from magnetic tension, which opposes the horizontal flow. The direction of flow reverses after half a cycle; an eastward azimuthal flow drives a meridional flow towards the Equator.

Braginsky[7] obtained analytical solutions for these waves when the radial magnetic field is approximated by an axial dipole. Different modes of oscillations are distinguished by the spatial pattern of radial flow. The gravest modes are associated with upwelling at the poles and downwelling at the Equator over half a cycle. For each pattern of radial flow there are overtones associated with shorter wavelengths in the radial direction. In general the overtones are more heavily damped than the fundamental modes. In addition, waves with a larger number of upwellings and downwellings have shorter periods.

A description of waves with a more general form of radial magnetic field requires a numerical solution. Indirect inferences from geodetic observations[18,19], as well as numerical geodynamo models[17], suggest that a large part of the radial magnetic field near the core–mantle boundary resides in wavelengths that are too small to detect at the Earth's surface. A simple, but plausible, description of the radial magnetic field at the core–mantle boundary assumes a random distribution. Because magnetic tension does not depend on the direction of the field, I can approximate the root-mean-square (r.m.s.) value of the radial magnetic field as a constant over the surface of the core. Changes in the radial magnetic field across the stratified layer are small when the layer is sufficiently thin.

Two parameters specify the waves when the r.m.s. value of the radial magnetic field is fixed by geodetic constraints at 0.6 mT (see Methods). One parameter is the thickness H of the stratified layer and the other is the buoyancy frequency N defined as

$$N = \sqrt{-\frac{g}{\rho}\frac{\partial \rho}{\partial r}}$$

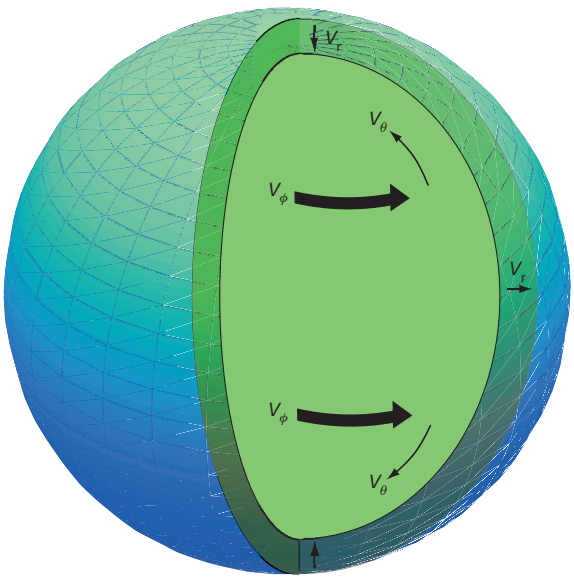

Figure 1 | Schematic illustration of the wave motion. Radial motion V_r causes a pressure perturbation, which drives an azimuthal flow V_ϕ in the stratified layer. The presence of a radial magnetic field opposes V_ϕ and induces a meridional flow V_θ. The fluid velocities reverse direction over a full cycle of the wave.

[1]Department of Earth and Planetary Science, University of California, Berkeley, California 94720, USA.

where $\rho \cong 10^4\ \mathrm{kg\,m^{-3}}$ is the fluid density, $\partial\rho/\partial r$ is the radial derivative and $g \cong 10\ \mathrm{m\,s^{-2}}$ is the acceleration due to gravity. Variations in density due to changes in hydrostatic pressure do not contribute to the buoyancy force, so the radial derivative in density is defined relative to variations in a well-mixed, isentropic fluid. For simplicity H is assumed to be constant and N varies linearly with radius across the layer. The value of N is largest at the core–mantle boundary and decreases to zero at the base of the stratified layer. As a result, the waves are completely defined by H and the maximum value of N (denoted as $N_{\max}$).

Figure 2 shows a representative wave with a symmetric pattern of upwelling and downwelling in the Northern and Southern hemispheres. This particular wave is computed using $H = 140$ km and ${N_{\max}}^2 = 1.02\Omega^2$, where $\Omega = 0.73 \times 10^{-4}\ \mathrm{s^{-1}}$ is the rotation rate of the planet. The corresponding period of the wave is 58 years, which is within the uncertainty of estimates for geomagnetic fluctuations.

The absolute amplitude of the wave in Fig. 2 is not uniquely set by the computations, but the relative size of the velocity components reveals the structure of the wave. The largest flow is associated with V_ϕ, whereas V_θ is about an order of magnitude smaller. Estimates of V_ϕ and V_θ have been inferred at the top of the core from variations in the geomagnetic field[8,9], so in principle we can look for evidence of wave motion in the surface core flow. The zonal part of V_ϕ (that is, independent of longitude) has a value of the order of several kilometres per year, and exhibits large variations in both space and time (see Fig. 3). On the other hand, the zonal part of V_θ is often prohibited by dynamical constraints in the inversion for flow[8,20]. Consequently, I begin my search for waves using only the zonal part of V_ϕ.

Estimates of V_ϕ over the time interval between 1930 and 1990 are well represented by a linear combination of waves. The chosen time interval is long enough to capture the dominant 60-year period, but restricts the record to times when the surface core flow is most reliable. Values for H and $N_{\max}$ are iteratively adjusted to minimize the misfit between the core-flow estimates and a linear combination of six MAC waves (see Extended Data Table 1). For each pair of model parameters (H, $N_{\max}$), the amplitude and phase of the waves are estimated by the method of least squares. The optimal fit to the core flow is shown in Fig. 3 using $H = 140$ km and ${N_{\max}}^2 = 1.02\Omega^2$. Good agreement means that the surface core flow is compatible with waves, but I cannot conclude that the wave motion uniquely accounts for the core flow.

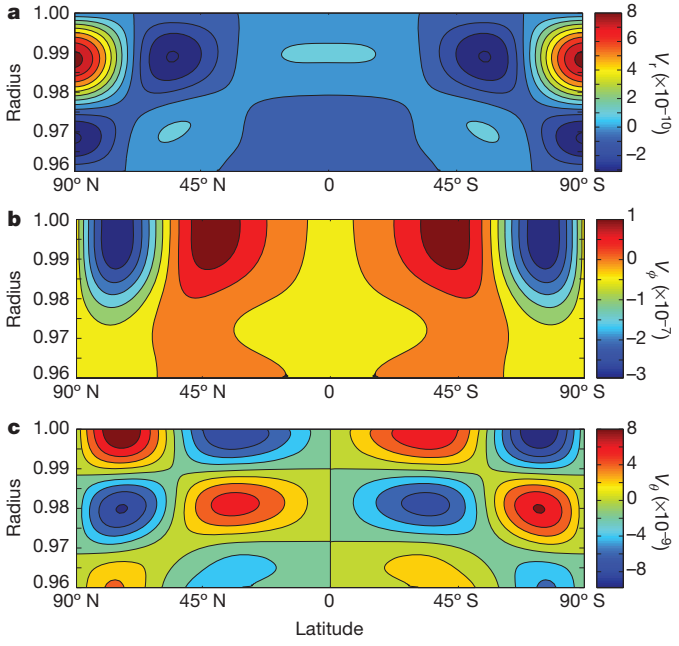

Figure 2 | A representative wave inside the stratified layer. The velocity components V_r (**a**), V_ϕ (**b**) and V_θ (**c**) are shown as a function of radius r and latitude, where $r = 1$ denotes the core–mantle boundary. This particular wave has a period of 58 years for the best-fitting values of layer thickness H and buoyancy frequency $N_{\max}$.

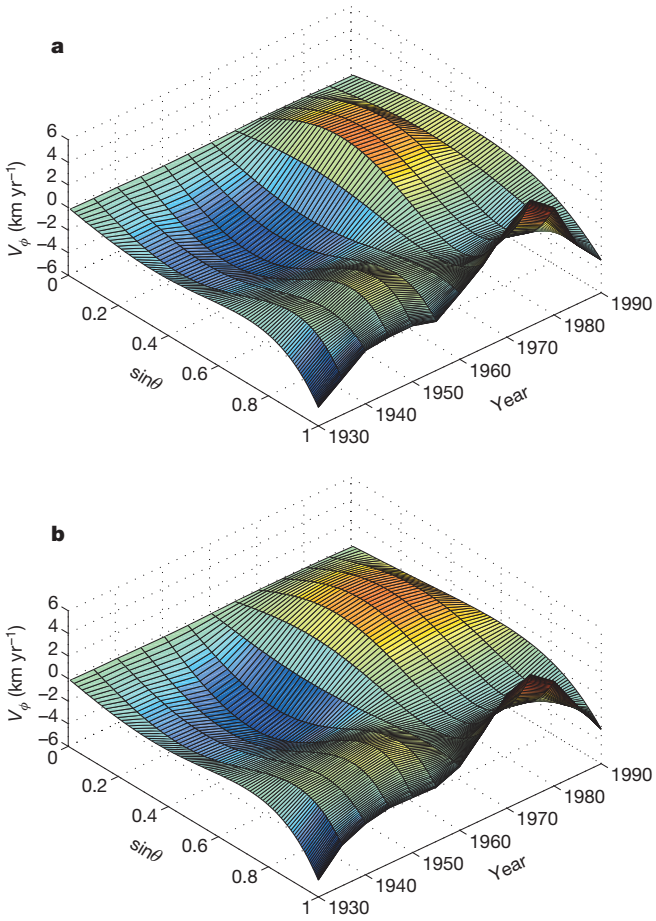

Figure 3 | Estimate of surface core flow and prediction due to MAC waves. **a**, Zonal flow V_ϕ from the uvm-s model of Jackson[8] is shown as a function of sinθ and time. Only the long-wavelength part of the flow in spherical harmonic degrees 1, 3 and 5 is retained for fitting the MAC waves. The components of the spherical harmonic expansion that are least affected are the small-scale flow and magnetic field at the core–mantle boundary[28]. **b**, A linear combination of six MAC waves can reliably reproduce the surface core flow. The model parameters for the waves (H, $N_{\max}$) are iteratively adjusted to find the optimal fit to the surface core flow.

An independent indication of wave motion is found in fluctuations of the dipole field[10]. Once a linear combination of waves is chosen to fit V_ϕ, the resulting V_θ component of flow alters the strength of the dipole field by sweeping the radial magnetic field into the polar regions. To quantify the changes in the dipole, I assume that the effects of magnetic diffusion are small for decadal fluctuations[20]. In this case time variations in the radial magnetic field B_r are described by

$$\dot{B}_r = -\nabla_H \cdot (\boldsymbol{V} B_r)$$

where ∇_H denotes the horizontal part of the divergence and $\boldsymbol{V}$ is the velocity due to waves. Only zonal components of B_r at the longest wavelengths contribute significantly to the dipole fluctuation because the waves are zonal and predominantly large-scale. When B_r is evaluated at the mid-range epoch of 1960 using the magnetic field model gufm1 (ref. 21), I obtain predictions for the fluctuation in the dipole field. Restoring the effects of magnetic diffusion causes only a small change in the amplitude and phase of the dipole fluctuation (see Methods). The resulting predictions are compared with time variations in the gufm1 model[21], after removing a linear trend in the strength of the dipole (Fig. 4).

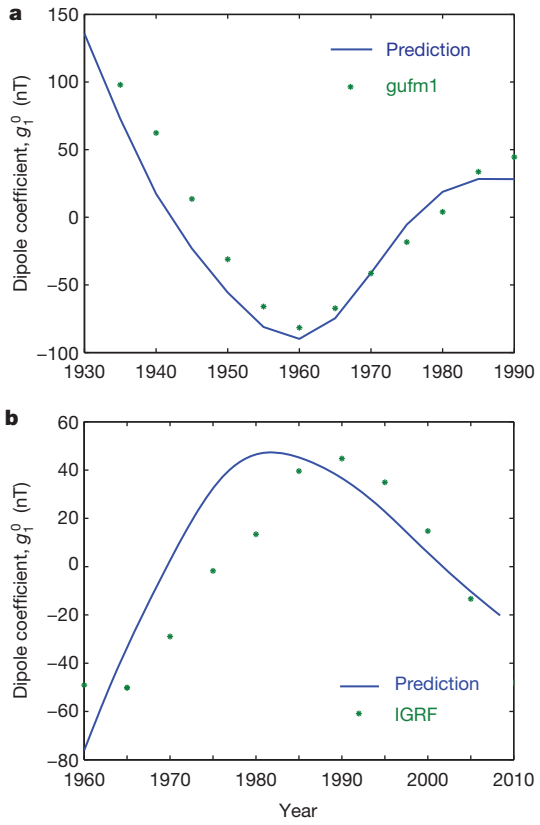

Figure 4 | Fluctuations in the dipole field due to MAC waves. Predictions for the interval 1930–1990 (**a**) and 1960–2008 (**b**) are based on the flow models of Jackson[8] and Wardinski and Lesur[22], respectively. The observed fluctuations are represented in terms of the Gauss coefficient $g_1^0(t)$ from the gufm1 model[21] and the IGRF model[29], after removing linear trends.

The amplitude and frequency of the dipole fluctuation agrees remarkably well with the prediction based on MAC waves. Even the decay of the dipole fluctuation is broadly consistent with the damping associated with the waves, although an excitation source must be present to sustain the waves over longer time intervals.

Evidence for MAC waves can also be found in more recent models of surface core flow. One example is the extended C^{3}FM model[22], which gives estimates for the flow between 1957 and 2008 from a combination of satellite and observatory observations. The set of waves that best fit the model of Jackson[8] also gives a good fit to the C^{3}FM model, although it is not possible to capture fluctuations with periods shorter than the shortest-period wave (see Methods). Slightly better fits to the C^{3}FM model are possible with a modest increase in stratification to $N_{max}{}^2 = 1.08\Omega^2$, but I retain the original set of waves to predict dipole fluctuations in more recent times. These predictions match the observations reasonably well with no adjustable parameters (see Fig. 4b).

Satisfactory predictions for the dipole fluctuations in Fig. 4 require an electrical conductivity of 10^6 S m^{-1}, which is consistent with recent theoretical predictions[11,12]. Lower values of electrical conductivity cause excessive damping of the waves. Adopting larger values for H can offset the excess damping, but thicker layers underestimate the amplitude of the dipole fluctuation. In addition, the model appears to require a fairly uniform r.m.s. radial magnetic field over the surface of the core. Calculations with a dipolar radial field alter the structure of the waves enough to prevent a good fit to both V_ϕ and the dipole fluctuation.

Stratification at the top of the core can arise in several ways. Thermal stratification is expected when the core heat flow is less than a hypothetical heat flow conducted through a well-mixed region at the top of the core[23,24] (sometimes called the adiabatic heat flow). A simple model for thermal stratification[25] suggests that a core heat flow of 13 TW would produce a stratified layer 140 km thick when the adiabatic heat flow is 15 TW (ref. 11). These two heat flows correspond to temperature gradients that differ by 0.12 K km^{-1}, yielding a density gradient of 0.012 kg km^{-1} at the core–mantle boundary. The resulting buoyancy frequency is 1.5Ω, which is close to the estimate recovered by fitting V_ϕ to MAC waves. Alternatively, the stratification might arise from radial variations in composition. Convection in the underlying region would probably provide a continuous source of excitation for the waves because buoyant parcels strike the base of the stratified layer. The resulting wave motion would obscure deeper motions in the core at periods of roughly a century and less.

METHODS SUMMARY

Numerical solutions for the waves are adapted from a numerical geodynamo model[26]. Perturbations in the velocity and magnetic fields are expanded in vector spherical harmonics using a truncation at degree $l = 40$. Both of these fields are defined on a radial grid with 200 equally spaced levels. Radial derivatives in the governing equations are represented by second-order finite differences. When the time dependence is periodic, the governing equations and boundary conditions (see Methods) yield an eigenvalue problem for the frequency and structure of the waves. Iterative solutions are obtained using an incomplete Arnoldi method[27]. The resulting waves are used to compute the associated fluctuations in the dipole field. The induction equation for the perturbation in the radial magnetic field at the core–mantle boundary is discretized in latitude and solved using the finite difference method. The dipole component is extracted using the orthogonality of spherical harmonics.

Online Content Any additional Methods, Extended Data display items and Source Data are available in the online version of the paper; references unique to these sections appear only in the online paper.

Received 1 November 2013; accepted 30 January; corrected online 26 March 2014 (see full-text HTML version for details).

1. Currie, R. G. Geomagnetic line spectra—2 to 70 years. *Astrophys. Space Sci.* **21,** 425–438 (1973).
2. Roberts, P. H., Yu, Z. J. & Russell, C. T. On the 60-year signal from the core. *Geophys. Astrophys. Fluid Dyn.* **101,** 11–35 (2007).
3. Jackson, L. P. & Mound, J. E. Geomagnetic variation on decadal time scales: what can we learn from empirical mode decomposition? *Geophys. Res. Lett.* **37,** L14307 (2010).
4. Finlay, C. C., Dumberry, M., Chulliat, A. & Pais, M. A. Short timescale core dynamics: theory and observation. *Space Sci. Rev.* **155,** 177–218 (2010).
5. Braginsky, S. I. Torsional magnetohydrodynamic vibrations in the Earth's core and variations in day length. *Geomagn. Aeron.* **10,** 1–10 (1970).
6. Gillet, N., Jault, D., Canet, E. & Fournier, A. Fast torsional waves and strong magnetic field with the Earth's core. *Nature* **465,** 74–77 (2010).
7. Braginsky, S. I. MAC-oscillations of the hidden ocean of the core. *J. Geomag. Geoelectr.* **45,** 1517–1538 (1993).
8. Jackson, A. Time dependency of tangentially geostrophic core surface motion. *Phys. Earth Planet. Inter.* **103,** 293–311 (1997).
9. Bloxham, J. & Jackson, A. Time-dependent mapping of the magnetic field at the core-mantle boundary. *J. Geophys. Res.* **97,** 19537–19563 (1992).
10. Yokoyama, Y. & Yukutake, T. Sixty-year variation in a time series of the geomagnetic gauss coefficients between 1910 and 1983. *J. Geomag. Geoelectr.* **43,** 563–584 (1991).
11. Pozzo, M. Davies, C. Gubbins, D. & Alfe, D. Thermal and electrical conductivity of iron at Earth's core conditions. *Nature* **485,** 355–358 (2012).
12. Pozzo, M., Davies, C., Gubbins, D. & Alfe, D. Transport properties for liquid silicon-oxygen-iron mixtures at Earth's core conditions. *Phys. Rev. B* **87,** 014110 (2013).
13. Buffett, B. A. & Seagle, C. T. Stratification at the top of the core due to chemical interaction with the mantle. *J. Geophys. Res.* **115,** B04407 (2010).
14. Gubbins, D. & Davies, C. J. The stratified layer at the core-mantle boundary caused by barodiffusion of oxygen, sulphur and silicon. *Phys. Earth Planet. Inter.* **215,** 21–28 (2013).
15. Zatman, S. & Bloxham, J. Torsional oscillations and the magnetic field within the Earth's core. *Nature* **388,** 760–763 (1997).
16. Buffett, B. A., Mound, J. E. & Jackson, A. Inversion of torsional oscillations for the structure and dynamics of Earth's core. *Geophys. J. Int.* **177,** 878–890 (2009).
17. Christensen, U. R. Geodynamo models: tools for understanding properties of Earth's magnetic field. *Phys. Earth Planet. Inter.* **187,** 157–169 (2011).
18. Buffett, B. A., Matthews, P. M. & Herring, T. A. Modeling of nutation and precession: effects of electromagnetic coupling. *J. Geophys. Res.* **107,** B42070 (2002).
19. Koot, L. *et al.* Constraints on the coupling at the core-mantle and inner-core boundaries inferred from nutation observations. *Geophys. J. Int.* **182,** 1279–1294 (2010).
20. Holme, R. & Olsen, N. Core surface flow modeling from high-resolution secular variation. *Geophys. J. Int.* **166,** 518–528 (2006).
21. Jackson, A., Jonkers, A. R. T. & Walker, M. R. Four centuries of geomagnetic secular variation from historical records. *Phil. Trans. R. Soc. Lond. A* **358,** 957–990 (2000).

22. Wardinski, I. & Lesur, V. An extended version of the C^3FM geomagnetic field model: application of a continuous frozen-flux constraint. *Geophys. J. Int.* **189,** 1409–1429 (2012).
23. Gubbins, D., Thomson, C. J. & Whaler, K. A. Stable regions in the Earth's liquid core. *Geophys. J. R. Astron. Soc.* **68,** 241–251 (1982).
24. Labrosse, S., Poirier, J. P. & LeMouel, J. L. On the cooling of the Earth's core. *Phys. Earth Planet. Inter.* **99,** 1–17 (1997).
25. Lister, J. R. & Buffett, B. A. Stratification of the outer core at the core-mantle boundary. *Phys. Earth Planet. Inter.* **105,** 5–19 (1998).
26. Kuang, W. & Bloxham, J. Numerical modeling of magnetohydrodynamic conv6ction in a rapidly rotating spherical shell: Weak and strong field dynamo action. *J. Comput. Phys.* **153,** 51–81 (1999).
27. Sorensen, D. C. Implicit application of polynomial filters in a k-step Arnoldi method. *SIAM J. Matrix Anal. Appl.* **13,** 357–385 (1992).
28. Eymin, C. & Hulot, G. On core surface flows inferred from satellite magnetic data. *Phys. Earth Planet. Inter.* **152,** 200–220 (2005).
29. Finlay, C. *et al.* International geomagnetic reference field: the eleventh generation. *Geophys. J. Int.* **183,** 1216–1230 (2010).

Acknowledgements A. Jackson and I. Wardinski provided models of surface core flow and magnetic field. Comments and suggestions from R. Holme substantially improved the final text. This work was supported in part by the US National Science Foundation (EAR-1045277).

Author Information Reprints and permissions information is available at www.nature.com/reprints. The authors declare no competing financial interests. Readers are welcome to comment on the online version of the paper. Correspondence and requests for materials should be addressed to B.B. (bbuffett@berkeley.edu).

METHODS

Description of waves. MAC waves can be represented by small perturbations in velocity $\boldsymbol{v}$ and magnetic field $\boldsymbol{b}$. These perturbations are superimposed on background fields $\boldsymbol{V}$ and $\boldsymbol{B}$, which are assumed to be steady over the period of the waves. I take $\boldsymbol{V}=0$ and confine my attention to the radial part of $\boldsymbol{B}$, which exerts the greatest influence on the waves. Braginsky[7] derived linearized equations for $\boldsymbol{v}$ and $\boldsymbol{b}$. I follow that treatment, but retain two additional terms. One is the local inertia and the other is the horizontal component of the mean rotation vector of the Earth (denoted by $\boldsymbol{\Omega}=\Omega\hat{\boldsymbol{z}}$, where $\hat{\boldsymbol{z}}$ is the unit vector in the polar direction).

The density perturbation $\Delta\rho$ in an incompressible fluid arises from displacement $\boldsymbol{u}$ through a density gradient $\nabla\rho$. To a good approximation the density gradient is radial, so I let

$$\Delta\rho=-\boldsymbol{u}\nabla\rho\approx-u_r\frac{\partial\rho}{\partial r}$$

For small-amplitude waves the displacement and velocity are related by

$$\partial\boldsymbol{u}/\partial t=\boldsymbol{v}$$

The governing equations for $\boldsymbol{v}$ and $\boldsymbol{b}$ can be written in non-dimensional form using the radius of the core R as the length scale, Ω^{-1} as the timescale and $(\Omega\rho\mu\eta)^{1/2}$ as the scale for the magnetic field. Here μ is the magnetic permeability and η is the magnetic diffusivity of the liquid core. The resulting dimensionless equations are

$$\partial\boldsymbol{v}/\partial t+2(\hat{\boldsymbol{z}}\times\boldsymbol{v})=-\nabla P+E_\eta(\nabla\times b)\times B-\tilde{N}^2(u\cdot\hat{\boldsymbol{r}})\hat{\boldsymbol{r}}+E\nabla^2\boldsymbol{v}$$

and

$$\partial\boldsymbol{b}/\partial t=\nabla\times(\boldsymbol{v}\times b)+E_\eta\nabla^2\boldsymbol{b}$$

where the dimensionless parameters are

$$\tilde{N}^2=\frac{N^2}{\Omega^2}$$

$$E=\frac{\nu}{\Omega R^2}$$

$$E_\eta=\frac{\eta}{\Omega R^2}$$

The first parameter is a dimensionless buoyancy frequency, whereas the second and third parameters characterize the influence of viscosity ν and magnetic diffusivity η, respectively. The velocity and magnetic fields also satisfy the solenoidal conditions $\nabla\cdot\boldsymbol{v}=\nabla\cdot\boldsymbol{b}=0$.

Solutions are subject to boundary conditions at the top and bottom of the stratified layer. The velocity perturbation satisfies viscous stress-free conditions at the top and bottom boundaries. In addition, the radial velocity vanishes at the core–mantle boundary. The flow below the stratified layer is expected to take the form of a torsional oscillation, which has a small radial component of motion. Consequently, I can reasonably assume that the radial velocity at the base of the stratified layer also vanishes. The magnetic field at the top of the layer is continuous with a potential field outside the core under the assumption that the mantle is an electrical insulator. Electromagnetic conditions at the base of the layer require continuity of both the radial magnetic field and the horizontal electric field. The magnetic perturbation below the stratified layer is obtained by solving the induction equation for $\boldsymbol{b}$, assuming that the amplitude of torsional oscillations at depth is small compared with the amplitude of MAC waves. Justification for these approximations is given below.

Numerical solution. Solenoidal conditions on $\boldsymbol{v}$ and $\boldsymbol{b}$ are imposed using a toroidal–poloidal decomposition that is commonly applied in numerical geodynamo models[26]. The toroidal and poloidal scalars are expanded in spherical harmonics with coefficients that depend on radius r and time t. Each coefficient corresponds to a particular degree l and order m in the spherical harmonic expansion. The time dependence for all coefficients (say t_l^m) is represented in the form

$$t_l^m(r,t)=\tilde{t}_l^m(r)e^{i\omega t}$$

where $\tilde{t}$ describes the radial dependence and ω is the frequency of the wave. Radial derivatives in the governing equations are approximated by second-order finite differences on an evenly spaced grid in radius.

Substituting the spherical harmonic expansions into the governing equations defines a system of algebraic equations of the form

$$A\mathbf{x}=\omega B\mathbf{x}$$

where $\boldsymbol{x}$ is a vector of scalar coefficients for $\boldsymbol{v}$, $\boldsymbol{b}$ and $\boldsymbol{u}$ at the radial grid points. Similarly, the boundary conditions can be written in matrix form as

$$Cx=0.$$

The governing equations and boundary conditions can be combined into a single matrix equation[30]

$$\begin{bmatrix}A & C^T\\ C & 0\end{bmatrix}\begin{bmatrix}\mathbf{x}\\ \epsilon\end{bmatrix}=\omega\begin{bmatrix}B & 0\\ 0 & 0\end{bmatrix}\begin{bmatrix}\mathbf{x}\\ \epsilon\end{bmatrix}$$

where $\boldsymbol{\varepsilon}$ are auxiliary variables, which tend to vanish as the resolution of the numerical solution improves. Iterative solutions for the complex eigenvalues ω are obtained using an incomplete Arnoldi method[27].

Numerical solutions are obtained on a radial grid with 200 levels. The spherical harmonic expansion is truncated at $l_{max}=40$. Solutions for zonal waves ($m=0$) fall into two classes, depending on whether the radial flow is symmetric or antisymmetric about the equator. I confine my attention to symmetric waves because the azimuthal flow inferred from secular variation[8] is primarily symmetric.

Treatment of the main magnetic field. Waves in a thin, stratified layer are affected by the radial component of the main magnetic field. Braginsky[7] obtained analytical solutions for waves when the radial magnetic field was approximated by a dipole. Geodetic constraints[18,19] and numerical geodynamo models[17] suggest that a large part of the field at the core–mantle boundary resides in multi-pole components with length scales that are too small to detect at the surface. This means that the main magnetic field cannot be inferred directly from surface observations. Fortunately, the waves are sensitive only to the amplitude of the radial field because magnetic tension is independent of the sign of the radial field. Geodetic constraints suggest that the r.m.s. value of the radial magnetic field is roughly 0.7 mT, assuming an electrical conductivity of $\sigma=5\times10^5\,\mathrm{S\,m^{-1}}$ on either side of the core–mantle boundary. High values on the mantle side might be attributed to the influence of liquid iron in the core, which is trapped by the effects of boundary topography when the top of the core is stratified[31]. In this case, an upward revision of electrical conductivity in liquid iron[11] would imply stronger electromagnetic coupling between the core and the mantle. Adopting a recently proposed estimate of $\sigma=10^6\,\mathrm{S\,m^{-1}}$ lowers the r.m.s. value of the radial magnetic field $B_r^{\mathrm{r.m.s.}}$ to approximately 0.6 mT. Assuming that the radial field is distributed randomly across a broad range of scales, I approximate $B_r^{\mathrm{r.m.s.}}$ as a constant over the core–mantle boundary.

A conductivity of $\sigma=10^6\,\mathrm{S\,m^{-1}}$ and a permeability of $\mu=4\pi\times10^{-7}\,\mathrm{H\,m^{-1}}$ gives a magnetic diffusivity of $\eta=1/\sigma\mu=0.8\,\mathrm{m^2\,s^{-1}}$. The characteristic magnetic field is $(\Omega\rho\mu\eta)^{1/2}=0.86$ mT, which implies a dimensionless radial main field of 0.7. Using $R=3.48\times10^6$ m and $\Omega=0.729\times10^{-4}\,\mathrm{s^{-1}}$ gives $E\eta=9\times10^{-10}$. I adopt a turbulent value for ν and let $E=E\eta$, although the resulting waves are relatively insensitive to the choice of E when stress-free boundary conditions are imposed.

Wave period and damping. The best fit of waves to estimates of surface core flow from Jackson[8] are obtained with a layer thickness of $H=140$ km and a stratification of $N^2=1.02\Omega^2$ at the core–mantle boundary. The resulting waves are classified according to the dominant spherical harmonic degree of the radial flow (denoted by L). I also distinguish between the fundamental mode $n=0$ and the first overtone $n=1$. Interestingly, the first overtones have lower frequencies than the corresponding fundamental modes. Higher overtones are heavily damped, which makes them less likely to be detected in surface observations. Extended Data Table 1 summarizes the period and the quality factor Q of the eight gravest modes. For present purposes the quality factor is approximated by

$$Q=\frac{\mathrm{Re}(\omega)}{2\,\mathrm{Im}(\omega)}$$

where Re and Im refer to the real and imaginary components of ω. The two longest-period waves at $L=2$ are omitted from the fit to the surface core flow, although the results are not substantially altered if these two long-period waves are included in the fit. The relative contribution of all eight waves, based on the r.m.s. value of V_ϕ, is listed in Extended Data Table 1.

Calculation of dipole fluctuations. Fluctuations in the radial magnetic field at the core–mantle boundary are described by

$$\partial b_r/\partial t=-\nabla_H\bullet(\boldsymbol{v}B_r)+\frac{\eta}{r}\nabla^2(rb_r)$$

where b_r is the radial fluctuation and B_r denotes the radial component of the main magnetic field. The first term on the right-hand side represents the advection of the main magnetic field by the waves, whereas the second term describes the effects of diffusion on the fluctuations. The primary contribution to the diffusion term comes from radial gradients in b_r, particularly when waves are confined to a thin stratified layer. For a characteristic radial length scale of H/π, the induction equation for b_r can be approximated by

$$\partial b_r/\partial t + \frac{\pi^2}{H^2} b_r = -\nabla_H(\boldsymbol{v} B_r)$$

Only zonal parts of B_r contribute to the fluctuations in the dipole field. I evaluate B_r on a grid in latitude using the gufm1 model[21]. Similarly, I evaluate $\boldsymbol{v}$ for each mode and compute the horizontal divergence using finite differences. A solution for b_r is obtained for each mode using the known frequency. A linear superposition of waves yields the complete time variation. The dipole component is recovered using the orthogonality of spherical harmonics.

Coupling to torsional oscillations. Wave motion in a stratified layer at the top of the core is coupled to flow in the deeper parts of the core. Such flow should be nearly geostrophic on timescales of several decades[32]. To investigate the nature of this coupling I extend the domain of the numerical model to include an unstratified region ($N^2 = 0$) below the layer that supports MAC waves. A constant main field $\boldsymbol{B} = B\hat{\boldsymbol{z}}$, is assumed throughout the domain. This particular choice of $\boldsymbol{B}$ allows wave motion to exert magnetic stresses on the underlying fluid. However, the resulting geostrophic flow does not support torsional oscillations because the background magnetic field does not cross fluid cylinders. Allowing for fast torsional oscillations[6] would tightly couple the fluid cylinders on decadal timescales. In this case I might approximate the underlying flow by assuming a rigid-body motion. Slower torsional oscillations with periods comparable to those of MAC waves would give rise to more complicated behaviour and would require a more comprehensive numerical treatment.

The extended calculation reveals that the strongest flow is confined to the stratified region at the top of the core (see Extended Data Fig. 1). A weaker flow is driven in the interior by magnetic stresses at the interface between stratified and unstratified regions. The direction of the deeper flow is opposite to that in the stratified layer, as expected on the grounds of angular momentum conservation. The amplitude of V_ϕ is quite small at the base of the stratified layer where the direction of flow changes sign. Allowing for fast torsional oscillations would probably reduce the amplitude of V_ϕ in the interior. In all cases the radial component of flow in the interior is weak (see Extended Data Fig. 2). These conditions are approximated in the calculation of isolated MAC waves by assuming that all components of $\boldsymbol{v}$ are small at the base of the stratified layer.

30. Fox, L. & Parker, I. B. *Chebyshev Polynomials in Numerical Analysis* (Oxford Univ. Press, 1968).
31. Buffett, B. A. Chemical stratification at the top of Earth's core: constraints from observations of nutations. *Earth Planet. Sci. Lett.* **296,** 367–372 (2010).
32. Jault, D. Axial invariance of rapidly varying diffusionless motion in the Earth's core interior. *Phys. Earth Planet. Inter.* **166,** 67–76 (2008).

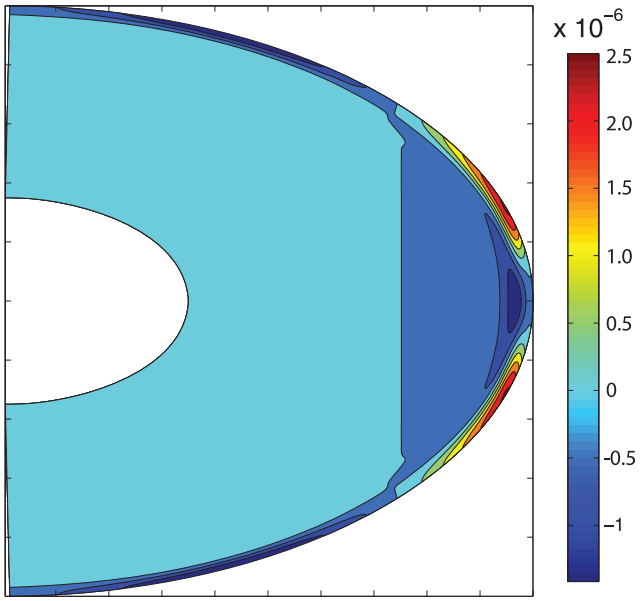

Extended Data Figure 1 | Azimuthal velocity V_ϕ on a meridional cross-section. Wave motion in the stratified layer at the top of the core induces geostrophic flow in the underlying fluid. The geostrophic nature of the deeper flow is inferred from the axial independence of the velocity.

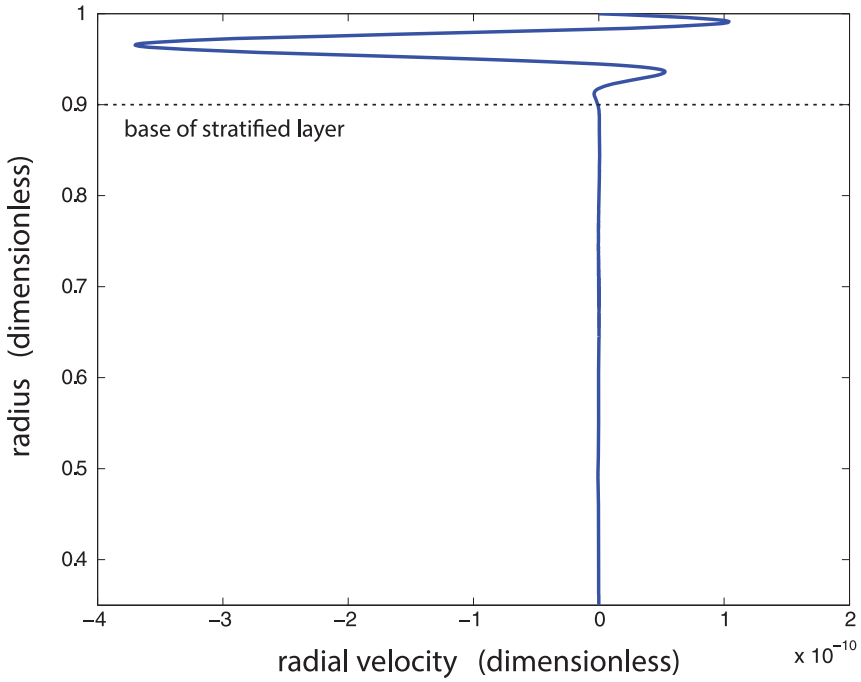

Extended Data Figure 2 | Radial velocity along a radial transect at colatitude $\theta = 40°$. Radial motion is confined to the stratified layer and vanishes in the nearly geostrophic interior.

Extended Data Table 1 | Period, quality factor and relative amplitude of the eight gravest modes

Mode L	Overtone n	Period (yr)	Q	Fit to Flow (%)
2	0	119	2.5	4.9
2	1	138	1.0	3.8
4	0	58	2.9	31.7
4	1	73	1.8	19.1
6	0	38	3.3	15.9
6	1	52	1.8	16.7
8	0	29	3.5	2.6
8	1	42	1.9	5.1